Compensation Method of Position Estimation Error for High-Speed Surface-Mounted PMSM Drives Based on Robust Inductance Estimation

Yao, Yu; Huang, Yunkai; Peng, Fei; Dong, Jianning; Zhu, Zichong

DOI
10.1109/TPEL.2021.3106510

Publication date
2022

Document Version
Final published version

Published in
IEEE Transactions on Power Electronics

Compensation Method of Position Estimation Error for High-Speed Surface-Mounted PMSM Drives Based on Robust Inductance Estimation

Yu Yao, *Student Member, IEEE*, Yunkai Huang, Fei Peng, *Member, IEEE*, Jianning Dong, *Member, IEEE*, and Zichong Zhu, *Student Member, IEEE*

***Abstract*—This article proposes a compensation method of position estimation error for high-speed surface-mounted permanent magnet synchronous motors based on robust inductance estimation. The proposed method relies on the variation of the estimated δ-axis back back-electromotive force when a small current is injected into the γ axis. The inductance estimation error is limited within $\pm 5\%$ when the nominal resistance and inductance vary $\pm 30\%$ of their real values. With the estimated inductance, the position estimation error can be well compensated. Compared with the conventional current-injection method, the proposed method has enhanced robustness against the system noises. Benefiting from this, it is effective to estimate the inductance with a small injected current (0.5% of the rated current), where the conventional methods fail. Finally, the effectiveness of the proposed method is validated by simulation and experiment results on a 100 kr/min (1.67 kHz) high-speed permanent magnet synchronous machines accurately with 10-kHz sampling frequency.**

***Index Terms*—High-speed permanent magnet synchronous machines (HSPMSM), inductance identification, position estimation error, small current injection.**

I. Introduction

HIGH-SPEED permanent magnet synchronous machines (HSPMSMs) are widely used in many applications because it has high power density, high efficiency, and free-gearbox drives [1]. In order to obtain high control performance, accurate rotor position information is essential in motor drives. However, the rotor position sensor on the high-speed shaft is often not welcome or not possible because of the cost requirement, limited space, and reliability consideration. Therefore, position sensorless control methods are extensively studied in HSPMSM drives.

Generally, the back-electromotive force (EMF) estimation methods are preferred for the high-speed position sensorless application. The estimation of back EMF can be developed in the stationary $\alpha\beta$ reference frame or in the estimated rotational $\gamma\delta$ coordinate based on motor models. According to the designed structure, the estimation methods mainly include the filter-based method [2], [3], sliding-mode methods [4]–[7], adaptive methods [8]–[11], and the extended Kalman filter methods [12], etc. But these conventional position sensorless methods of PMSM are often implemented based on the forward Euler discretization, which requires a reasonably high sampling frequency. The operating frequency of the HSPMSM is high because of high speed, while the switching and sampling frequency of the power converter is limited by the power semiconductor losses, analog-digital conversion delay, and microcontroller unit capability. As a consequence, the number of control actions per control period in the HSPMSM drive is limited. Conventional forward Euler-based methods may fail because of inaccuracy and instability [13].

To solve the aforementioned problem, several sensorless methods are established based on a discrete-time model with zero-order hold discretized. A fully discretized back-EMF estimation method based on the exact discrete-time model was proposed in [14] and [15], which pushed the sampling/fundamental frequency ratio to 6. In [16], a speed-adaptive full-order observer in the discrete-time domain is developed and tested, showing significant performance improvements when the sampling/fundamental frequency ratio is below 10. However, these position sensorless control methods are based on accurate models of HSPMSM, which requires accurate motor parameters, especially the inductances. Moreover, the robustness of the proposed methods against parameter variations are not provided.

Online parameter identification has been investigated in many literatures. Most of these methods are based on applications with rotor position sensors [17]–[23]. Some researches are carried out for the sensorless motor drives. Considering the well-known rank-deficient problem, some papers assumes that some parameters are regarded as accurate and the remaining electrical parameters are selected to be estimated [24], [25]. [24] estimates the winding resistance and dq-axis inductance while the PM flux linkage has to be known. In [25], the resistance and the

Manuscript received March 30, 2021; revised June 6, 2021 and July 15, 2021; accepted August 17, 2021. Date of publication August 20, 2021; date of current version October 15, 2021. This work was supported in part by the National Natural Science Foundation of China under Grant 51777034 and Grant 51707037, and in part by the Excellence Project Funds of Southeast University. Recommended for publication by Associate Editor I. Slama-Belkhodja. *(Corresponding author: Yunkai Huang.)*

Yu Yao, Yunkai Huang, and Fei Peng are with the School of Electrical Engineering, Southeast University, Nanjing 210096, China (e-mail: yuyao@seu.edu.cn; huangyk@seu.edu.cn; pengfei@seu.edu.cn).

Zichong Zhu is with the School of Electrical Engineering and Control Science, Nanjing Tech University, Nanjing 211800, China (e-mail: zichong_zhu@seu.edu.cn).

Jianning Dong is with the Delft University of Technology, 2628, CD Delft, Netherlands (e-mail: j.dong-4@tudelft.nl).

Color versions of one or more figures in this article are available at https://doi.org/10.1109/TPEL.2021.3106510.

Digital Object Identifier 10.1109/TPEL.2021.3106510

flux linkage are estimated online while the stator inductance is treated as a known parameter. Several methods can achieve parameter identification without this assumption [26]–[28]. But the experimental results indicate the estimated parameters did not converge to their real values and the position estimation error is still unacceptably large.

Another popular solution to the rank-deficient problem is current-injection methods [29]–[31]. With the current injection, the voltage equations are full-ranked and the system parameters can be calculated by the recursive least square or other numerical approaches. The current is usually injected into the direct axis and there is a tradeoff on the amplitude selection. On one hand, the amplitude should be as small as possible to reduce the effects on the inductance saturation. On the other hand, the amplitude of the current injection has to be adequately large to improve the ratio of signal versus noises. Among these methods, the injected current is up to 50% of the rated current in [29], 5% of the rated current in [30], and 13.3% of the rated current in [31]. Therefore, it is significant to enhance the robustness against the system noises, and thus, reduce the amplitude of the injected current. Besides, it is worth noting that these methods are still proposed based on the continuous-time model or approximate discrete-time model using the forward-Euler method. For the sensorless drive of HSPMSMs with the sampling/fundamental frequency ratio down to 6, the discrete-time model is more complicated and these methods are also not applicable.

To solve the aforementioned problems, a robust inductance estimation method for EMF-based position sensorless drive of HSPMSMs is proposed by using a small current injection. There are some achievements as follows.

1) The inductance estimation error is limited within $\pm 5\%$ of the real value when the nominal resistance and inductance vary $\pm 30\%$. With the estimated inductance, the position estimation error can be well compensated.
2) Compared with the traditional current injection-based method [29]–[31], the proposed method has enhanced robustness against the system noises. As a consequence, it is effective to estimate the inductance with a small injected current (0.5% of the rated current), where the conventional methods fail.
3) Because of the fully discretized design, the proposed method can be used under the low sampling/fundamental frequency ratio (down to 6).

Finally, the proposed method is validated by both simulation and experimental results on a 100-kr/min motor with 10-kHz sampling frequency.

II. Discrete-Time Model and EMF-Based Position Estimation of HSPMSM

A. Discrete-Time Model

According to [14], the discrete-time model in the estimated $\gamma\delta$ reference frame is derived as

$$\begin{aligned}\mathbf{i}_{\gamma\delta}(k+1) &= \mathbf{G}\mathbf{i}_{\gamma\delta}(k) + \mathbf{H}\mathbf{v}_{\gamma\delta}(k) + \mathbf{F}\mathbf{e}_{\gamma\delta}(k)\\ \mathbf{i}_{\gamma\delta} &= [i_\gamma\ i_\delta]^T\\ \mathbf{v}_{\gamma\delta} &= [v_\gamma\ v_\delta]^T\\ \mathbf{e}_{\gamma\delta} &= \omega\Psi[-\sin\tilde{\theta}_e\ \cos\tilde{\theta}_e]^T\end{aligned} \tag{1}$$

where $\mathbf{i}_{\gamma\delta}$ is the winding current. $\mathbf{v}_{\gamma\delta}$ denotes the inverter output voltage. $\mathbf{e}_{\gamma\delta}$ refers to the back EMF. ω is the angular speed and Ψ denotes the PM flux linkage. $\tilde{\theta}_e$ is the position estimation error. The matrices are defined as

$$\begin{aligned}&\mathbf{G} = \mathbf{T}_w\mathbf{G}_1 \quad \mathbf{H} = \mathbf{T}_w\mathbf{H}_1 \quad \mathbf{F} = \mathbf{T}_w\mathbf{G}_2\\ &\mathbf{T}_w = \begin{bmatrix}\cos(\omega(k)T) & \sin(\omega(k)T)\\ -\sin(\omega(k)T) & \cos(\omega(k)T)\end{bmatrix}\\ &\mathbf{G}_1 = x\begin{bmatrix}1 & 0\\ 0 & 1\end{bmatrix} \quad \mathbf{G}_2 = \begin{bmatrix}d_1 & -d_2\\ d_2 & d_1\end{bmatrix} \quad \mathbf{H}_1 = y\begin{bmatrix}1 & 0\\ 0 & 1\end{bmatrix}\\ &d_1 = \frac{(x-\cos(\omega T))R - \sin(\omega T)\omega L}{R^2+\omega^2L^2}\\ &d_2 = -\frac{(x-\cos(\omega T))\omega L + \sin(\omega T)R}{R^2+\omega^2L^2}\\ &x = e^{-\frac{R}{L}T} \quad y = \frac{1-e^{-\frac{R}{L}T}}{R}\end{aligned} \tag{2}$$

where the T is the sampling period. R is the stator resistance, L is the stator inductance. d_1 and d_2 are the coefficients of the back EMF.

B. Sliding-Mode Disturbance Observer

For the position sensorless drive of the HSPMSM, the estimation of the back EMF is widely used, which can be easily achieved by a model-based observer. Generally, considering the parameters mismatch, there is

$$\hat{R} \neq R \quad \hat{L} \neq L \tag{3}$$

where the $\hat{R}$ and $\hat{L}$ are the nominal values of the resistance and the inductance, respectively. Based on the model (1), the discrete-time back-EMF observer can be written as

$$\hat{\mathbf{i}}_{\gamma\delta}(k+1) = \hat{\mathbf{G}}\hat{\mathbf{i}}_{\gamma\delta}(k) + \hat{\mathbf{H}}\mathbf{v}_{\gamma\delta}(k) + \hat{\mathbf{F}}\hat{e}_{\gamma\delta}(k) \tag{4}$$

where $\hat{\mathbf{G}}$, $\hat{\mathbf{H}}$, and $\hat{\mathbf{F}}$ are the matrices with respect to $\hat{R}$ and $\hat{L}$. $\hat{\mathbf{e}}_{\gamma\delta}$ is the estimated back EMF.

By subtracting (1) from (4), it can be derived that

$$\tilde{\mathbf{i}}_{\gamma\delta}(k+1) = \hat{\mathbf{G}}\tilde{\mathbf{i}}_{\gamma\delta}(k) + \hat{\mathbf{F}}\hat{e}_{\gamma\delta}(k) - \mathbf{p}(k) \tag{5}$$

and

$$\mathbf{p}(k) = \mathbf{F}\mathbf{e}_{\gamma\delta}(k) - (\hat{\mathbf{G}}-\mathbf{G})\mathbf{i}_{\gamma\delta}(k) - (\hat{\mathbf{H}}-\mathbf{H})\mathbf{v}_{\gamma\delta}(k)$$

where the $\tilde{\mathbf{i}}_{\gamma\delta}$ denotes the current estimation error vector.

In order to make $\tilde{\mathbf{i}}_{\gamma\delta}(k)$ converge to zero, the The attraction function of $\hat{\mathbf{e}}(k)$ is designed as

$$\hat{\mathbf{e}}_{\gamma\delta}(k) = \hat{\mathbf{F}}^{-1}\left(\lambda\tilde{\mathbf{i}}_{\gamma\delta}(k) - \hat{\mathbf{G}}\tilde{\mathbf{i}}_{\gamma\delta}(k) + \hat{\mathbf{p}}(k)\right) \tag{6}$$

and the $\hat{\mathbf{p}}(k)$ is the time-delay disturbance estimation as

$$\hat{\mathbf{p}}(k) = \hat{\mathbf{G}}\tilde{\mathbf{i}}_{\gamma\delta}(k-1) + \hat{\mathbf{F}}\hat{e}_{\gamma\delta}(k-1) - \tilde{\mathbf{i}}_{\gamma\delta}(k) \tag{7}$$

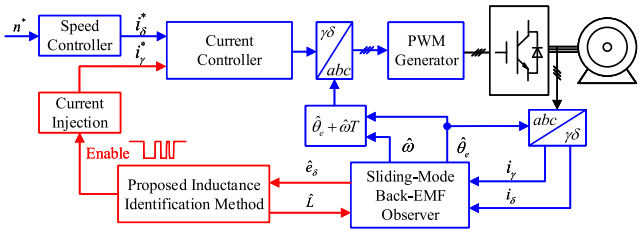

Fig. 1. System diagram of the proposed identification method.

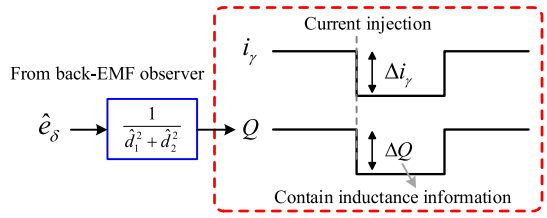

Fig. 2. Principle of the proposed identification method.

where the λ is a positive constant. When $\lambda \in (0\ 1)$, it can be proved that the sliding-mode observer is stable [15]. When the current estimation error (i.e., $\tilde{\mathbf{i}}_{\gamma\delta}$) converges to zero, the estimation of the back EMF is

$$\hat{\mathbf{e}}_{\gamma\delta}(k) = \hat{\mathbf{F}}^{-1}\begin{pmatrix}\mathbf{F}\mathbf{e}_{\gamma\delta}(k) - (\hat{\mathbf{G}} - \mathbf{G})\mathbf{i}_{\gamma\delta}(k) \\ -(\hat{\mathbf{H}} - \mathbf{H})\mathbf{v}_{\gamma\delta}(k)\end{pmatrix}. \tag{8}$$

It is worth noting that the estimated back EMF will be deviated from the real values because of the mismatched parameters, especially the mismatched inductance. In that case, the position estimation error inevitably occurs, and thus, it is necessary to achieve online inductance estimation aiming at compensating the position estimation error.

III. Proposed Inductance Identification Method

Based on (8), it indicates that the mismatched parameters will inevitably cause the estimation error of rotor position when a model-based observer is implemented. Assuming that ω is obtained accurately, there is

$$\begin{aligned}\hat{e}_\gamma(k) &= \frac{P}{\hat{d}_1^2 + \hat{d}_2^2} \quad \hat{e}_\delta(k) = \frac{Q}{\hat{d}_1^2 + \hat{d}_2^2} \\ P &= (\hat{d}_1 d_1 + \hat{d}_2 d_2)e_\gamma(k) + (-\hat{d}_1 d_2 + \hat{d}_2 d_1)e_\delta(k) \\ &\quad - \hat{d}_1(\tilde{x}i_\gamma(k) + \tilde{y}v_\gamma(k)) - \hat{d}_2(\tilde{x}i_\delta(k) + \tilde{y}v_\delta(k)) \\ Q &= (-\hat{d}_2 d_1 + \hat{d}_1 d_2)e_\gamma(k) + (\hat{d}_2 d_2 + \hat{d}_1 d_1)e_\delta(k) \\ &\quad + \hat{d}_2(\tilde{x}i_\gamma(k) + \tilde{y}v_\gamma(k)) - \hat{d}_1(\tilde{x}i_\delta(k) + \tilde{y}v_\delta(k))\end{aligned} \tag{9}$$

where

$$\begin{aligned}\tilde{x} &= \hat{x} - x = e^{-\frac{\hat{R}}{\hat{L}}T} - e^{-\frac{R}{L}T} \\ \tilde{y} &= \hat{y} - y = \frac{1 - e^{-\frac{\hat{R}}{\hat{L}}T}}{\hat{R}} - \frac{1 - e^{-\frac{R}{L}T}}{R}.\end{aligned} \tag{10}$$

where $\hat{x}$, $\hat{y}$, $\hat{d}_1$, and $\hat{d}_2$ are nominal values of x, y, d_1, and d_2, respectively.

Fig. 2 shows the principle of the proposed method, which is based on the variation of Q (from the estimated back-EMF $\hat{e}_\delta$) when a current is injected into γ axis.

A. Variation of Q With Current Injection

The variation of the $\hat{e}_\delta$ with current injection into γ axis is analyzed. As it mentioned above, the speed stay unchanged after injection.

From (9), at time t_0, there is

$$\begin{aligned}Q_{t_0} &= (-\hat{d}_2 d_1 + \hat{d}_1 d_2)e_\gamma(t_0) + (\hat{d}_2 d_2 + \hat{d}_1 d_1)e_\delta(t_0) \\ &\quad + \hat{d}_2(\tilde{x}i_\gamma(t_0) + \tilde{y}v_\gamma(t_0)) - \hat{d}_1(\tilde{x}i_\delta(t_0) + \tilde{y}v_\delta(t_0)).\end{aligned} \tag{11}$$

A stepping current is then injected into the γ axis. After the control system back to steady state again at time t_1, it can be obtained that

$$\begin{aligned}rQ_{t_1} &= (-\hat{d}_2 d_1 + \hat{d}_1 d_2)e_\gamma(t_1) + (\hat{d}_2 d_2 + \hat{d}_1 d_1)e_\delta(t_1) \\ &\quad + \hat{d}_2(\tilde{x}i_\gamma(t_1) + \tilde{y}v_\gamma(t_1)) - \hat{d}_1(\tilde{x}i_\delta(t_1) + \tilde{y}v_\delta(t_1)).\end{aligned} \tag{12}$$

Subtracting (11) from (12), there is

$$\begin{aligned}\Delta Q = &\underbrace{(-\hat{d}_2 d_1 + \hat{d}_1 d_2)\Delta e_\gamma + (\hat{d}_2 d_2 + \hat{d}_1 d_1)\Delta e_\delta}_{We} \\ &\underbrace{+ \hat{d}_2(\tilde{x}\Delta i_\gamma + \tilde{y}\Delta v_\gamma) - \hat{d}_1(\tilde{x}\Delta i_\delta + \tilde{y}\Delta v_\delta)}_{W_L}\end{aligned} \tag{13}$$

where Δ refers to the difference between t_1 and t_0.

Lemma 1: For the high-speed machine, the winding resistance R, the stator inductance L, the electric angular speed ω, the sampling period T satisfies

$$\begin{aligned}R &< 0.2\omega L \\ RT &< 0.1L.\end{aligned} \tag{14}$$

This condition will be used to simplify the theoretical analysis and guarantee the estimation error boundary of the proposed method.

1) Characteristic of W_L: According to *Lemma 1*, the R can be neglected compared with ωL and there is

$$d_1 \approx -\frac{\sin(\omega T)}{\omega L} \quad d_2 \approx \frac{\cos(\omega T) - x}{\omega L}. \tag{15}$$

After the current injection, there is

1) the ω is unchanged after the injection with the help of the speed controller;
2) because of the injected current is much smaller than the rated current, the variation of the δ-axis current is neglected.

Based on these considerations and the discrete-time model (1), it can be derived as

$$\Delta v_\gamma = \frac{1}{y}(\cos(\omega T) - x)\Delta i_\gamma$$
$$\Delta v_\delta = \frac{1}{y}\sin(\omega T)\Delta i_\gamma. \tag{16}$$

Substituting (16) and (15) into W_L, there is

$$\begin{aligned} W_L &= \hat{d}_2\left(\tilde{x}\Delta i_\gamma + \tilde{y}\frac{1}{y}\left(\cos(\omega T) - x\right)\Delta i_\gamma\right) \\ &\quad - \hat{d}_1\tilde{y}\frac{1}{y}\sin(\omega T)\Delta i_\gamma \\ &= \frac{\left(\cos(\omega T) - \hat{x}\right)\omega\hat{L} - \sin(\omega T)\hat{R}}{\hat{R}^2 + \omega^2\hat{L}^2}\tilde{x}\Delta i_\gamma \\ &\quad + \frac{\left(\cos(\omega T) - \hat{x}\right)\left(\cos(\omega T) - x\right)\omega\hat{L}}{\hat{R}^2 + \omega^2\hat{L}^2}\frac{\tilde{y}}{y}\Delta i_\gamma \\ &\quad - \tilde{x}\frac{\sin(\omega T)\hat{R}}{\hat{R}^2 + \omega^2\hat{L}^2}\frac{\tilde{y}}{y}\Delta i_\gamma + \frac{\sin^2(\omega T)\omega\hat{L}}{\hat{R}^2 + \omega^2\hat{L}^2}\frac{\tilde{y}}{y}\Delta i_\gamma \end{aligned} \tag{17}$$

and by simplifying above equation, By applying Taylor expansion, there is

$$\begin{aligned} y &= \frac{1 - e^{-\frac{R}{L}T}}{R} \approx \frac{T}{L} \\ \hat{y} &= \frac{1 - e^{-\frac{\hat{R}}{\hat{L}}T}}{\hat{R}} \approx \frac{T}{\hat{L}} \\ \tilde{y} &= \hat{y} - y \approx \frac{T}{\hat{L}} - \frac{T}{L} = \frac{L - \hat{L}}{L\hat{L}}T \end{aligned} \tag{18}$$

and it leads to

$$\begin{aligned} W_L &= \frac{\left(\cos(\omega T) - \hat{x}\right)^2 + \sin^2(\omega T)}{\hat{R}^2 + \omega^2\hat{L}^2}\omega\left(L - \hat{L}\right)\Delta i_\gamma \\ &\quad + \frac{\left(\cos(\omega T) - \hat{x}\right)\omega\hat{L} - \sin(\omega T)\hat{R}}{\hat{R}^2 + \omega^2\hat{L}^2}\tilde{x}\Delta i_\gamma \\ &\quad + \tilde{x}\frac{\left(\cos(\omega T) - \hat{x}\right)\omega\hat{L} - \sin(\omega T)\hat{R}}{\hat{R}^2 + \omega^2\hat{L}^2}\frac{L - \hat{L}}{\hat{L}}\Delta i_\gamma. \end{aligned} \tag{19}$$

From the observation of (19), the W_L contains the information of the deviation between the real inductance and the nominal inductance.

2) Characteristic of W_e: The W_e can be expanded on basis of (13) as

$$\begin{aligned} W_e &= (-\hat{d}_2 d_1 + \hat{d}_1 d_2)\omega\Psi(\sin\tilde{\theta}_e(t_0) - \sin\tilde{\theta}_e(t_1)) \\ &\quad + (\hat{d}_2 d_2 + \hat{d}_1 d_1)\omega\Psi(\cos\tilde{\theta}_e(t_1) - \cos\tilde{\theta}_e(t_0)). \end{aligned} \tag{20}$$

Based on the equation above, the W_e is closely related with the variation of the position estimation error (i.e., $\Delta\tilde{\theta}_e$) when the γ-axis current is injected.

Fig. 3 shows the $\Delta\tilde{\theta}_e$ with Δi_γ (-1 to 1 A) injected and L varying from 0.5 to 1.5 L. It can be observed that the $\Delta\tilde{\theta}_e$ approximately stays unchanged, which means the injected current has negligible effects on the position estimation error. It can be concluded that the W_e is much smaller compared with the W_L. It indicates $\Delta Q \approx W_L$ holds when the current is injected into the γ axis and the speed stays unchanged with the speed controller.

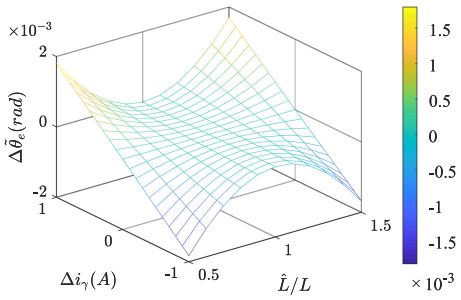

Fig. 3. $\Delta\tilde{\theta}_e$ with Δi_γ ranging from -1 to 1 A at 100 kr/min.

B. Proposed Identification Method and Error Analysis

The inductance deviation estimation is designed as

$$\Delta\hat{L} = \frac{\Delta Q}{\eta} \tag{21}$$

where the $\Delta\hat{L}$ is the estimation value of the $L - \hat{L}$. The η can be calculated directly in the digital implementation and is defined as

$$\eta = \frac{\left(\cos(\omega T) - \hat{x}\right)^2 + \sin^2(\omega T)}{\hat{R}^2 + \omega^2\hat{L}^2}\omega\Delta i_\gamma. \tag{22}$$

As the analysis mentioned above, the $\Delta Q \approx W_L$ holds. Bear this in mind, the inductance deviation estimation can be simplified as

$$\Delta\hat{L} = \frac{W_L}{\eta}. \tag{23}$$

The estimation error of the inductance deviation is evaluated and the following proposition holds.

Proposition: With the proposed estimation method (21) and $Lemma1$, when the parameters vary $\pm 30\%$ of their real values, the estimation error of the inductance deviation is obtained as

$$-0.023/\hat{x} < \Delta\hat{L} - \left(L - \hat{L}\right) < 0.0429\, L/\hat{x}. \tag{24}$$

Proof: From (19), there is

$$\Delta\hat{L} = \left(L - \hat{L}\right) + \rho\tilde{x}L \tag{25}$$

where the coefficient ρ is defined as

$$\rho = \frac{\left(\cos(\omega T) - \hat{x}\right)\omega\hat{L} - \sin(\omega T)\hat{R}}{\left(\cos(\omega T) - \hat{x}\right)^2 + \sin^2(\omega T)}\frac{1}{\omega\hat{L}}. \tag{26}$$

According to the Taylor series, there is

$$\begin{aligned} \hat{x} &\approx 1 - \frac{\hat{R}}{\hat{L}}T \\ \cos(\omega T) &\approx 1 - \frac{\omega^2 T^2}{2} \quad \sin(\omega T) \approx \omega T - \frac{\omega^3 T^3}{6} \end{aligned} \tag{27}$$

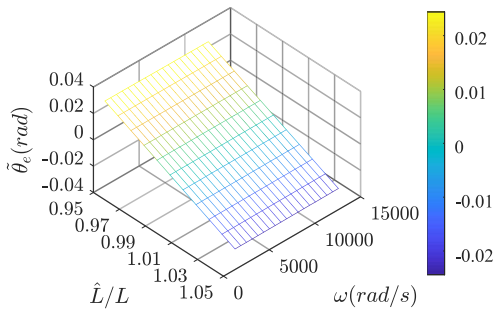

Fig. 4. $\Delta\tilde{\theta}_e$ with $\hat{L}$ ranging from -0.95 to $1.05\,L$.

and the coefficient ρ can be simplified as

$$\rho \approx \frac{\omega^2 T^2\left(\hat{R}T - 3\hat{L}\right)}{6\omega^2 T^2\hat{x} + 6(\hat{x}-1)^2}\frac{1}{\hat{L}}. \tag{28}$$

Generally, $\hat{R}T < 3\hat{L}$ always holds, which leads to

$$\rho > \frac{-\omega^2 T^2\left(3\hat{L}\right)}{6\omega^2 T^2\hat{x} + 6(\hat{x}-1)^2}\frac{1}{\hat{L}}. \tag{29}$$

Considering $6(\hat{x}-1)^2 > 0$, there is $-\frac{1}{2\hat{x}} < \rho < 0$.
For the item $\tilde{x}$

$$\tilde{x} \approx \frac{RT}{L} - \frac{\hat{R}T}{\hat{L}}. \tag{30}$$

In that case

$$\tilde{x}L \approx RT\left(1 - \frac{K_R}{K_L}\right) \tag{31}$$

where the $K_R = \hat{R}/R$ and $K_L = \hat{L}/L$. When the parameters vary $\pm 30\%$ of their real values, the $K_R \in [0.71.3]$ and $K_L \in [0.71.3]$, which leads to

$$-\frac{6}{7} < 1 - \frac{K_R}{K_L} < \frac{6}{13} \tag{32}$$

and there is

$$-\frac{6}{7}RT < \tilde{x}L < \frac{6}{13}RT. \tag{33}$$

According to *Lemma 1*, the boundary of $\tilde{x}L$ is derived as

$$-\frac{0.6}{7}L < \tilde{x}L < \frac{0.6}{13}L. \tag{34}$$

Therefore

$$-\frac{0.3}{13\hat{x}}L < \rho\tilde{x}L < \frac{0.3}{7\hat{x}}L. \tag{35}$$

This completes the proof.

It should be noted that this is a general conclusion for HSPMSMs with *Lemma 1* satisfied. Because the $\hat{x}$ is usually between 0.8 and 1, the estimation error boundary of the proposed method is less than $5\%L$. In that case, the position estimation error can be much reduced and close to zero, as shown in Fig. 4.

IV. Digital Implementation and Comparison With Conventional Method

A. Implementation Condition of Proposed Method

Based on the proposed inductance estimation method, a current should be injected into the γ axis. Considering the limited voltage margin and the torque ripple, the amplitude of injected current should be selected as small as possible

$$|\Delta i_\gamma| < 2\% I_N \tag{36}$$

where the I_N is the rated current. To eliminate the effects of the system noise, a threshold is adopted and the ΔQ should be

$$|\Delta Q| > Th. \tag{37}$$

Without loss of generality, the $Th.$ is 0.02. Additionally, the estimation error boundary is limited as

$$|L - \hat{L}| < 0.05\hat{L}. \tag{38}$$

Therefore, based on (21), the following equation should be satisfied as:

$$\varphi = \frac{(\cos(\omega T) - \hat{x})^2 + \sin^2(\omega T)}{\hat{R}^2 + \omega^2\hat{L}^2}\omega > \frac{20}{\hat{L}I_N}. \tag{39}$$

It is the implementation condition of the proposed identification method. It can be checked that this condition is satisfied in [32] and [33].

If the condition (39) holds, the amplitude of the injected current should be selected as

$$\frac{0.4}{\varphi\hat{L}} < |\Delta i_\gamma| < 2\% I_N. \tag{40}$$

Besides, considering the voltage margin, $\Delta i_\gamma < 0$, which indicates the current is injected into the negative γ axis.

B. Effect of the VSI Nonlinearity

Considering the voltage-source-inverter (VSI) dead time, the real voltage applied in the motor can be derived as [34]

$$\begin{aligned} v_\gamma^r(k) &= v_\gamma(k) + D_\gamma(k)V_{\text{dead}}(k) \\ v_\delta^r(k) &= v_\delta(k) + D_\delta(k)V_{\text{dead}}(k) \end{aligned} \tag{41}$$

where the $V_{\text{dead}} = \frac{T_{\text{off}} - T_{on} - T_d}{T}V_{dc} - V_{ce0} - V_{d0}$. T_{on}, T_{off}, T_d, V_{ce0}, and V_{d0} denote the switch ON time delay, the switch OFFtime delay, the dead time delay, voltage drops, and freewheeling diode. $D_\gamma(k)$ and $D_\delta(k)$ are

$$\begin{bmatrix} D_\gamma \\ D_\delta \end{bmatrix} = \mathbf{T}_{\text{abc2}\gamma\delta}\begin{bmatrix} \text{sign}(i_a) \\ \text{sign}(i_b) \\ \text{sign}(i_c) \end{bmatrix} \tag{42}$$

where the sign() denotes the sign function and $i_{a,b,c}$ represents the phase current. $\mathbf{T}_{\text{abc2}\gamma\delta}$ represents the transform matrix from the natural coordinate to the estimated $\gamma\delta$ coordinate. Fig. 5 shows the waveforms of the D_γ and D_δ when the fundamental frequency is 1000 Hz. It can be checked that the D_γ and D_δ are six-times fundamental-frequency components.

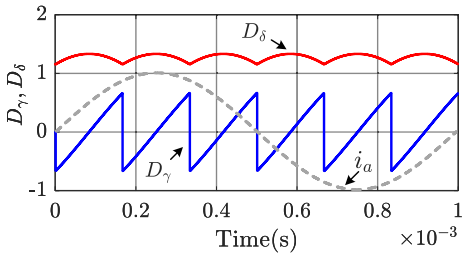

Fig. 5. D_γ and D_δ when the current frequency is 1000 Hz.

Considering the voltage distortion of the dead time, the Q can be rewritten as

$$\begin{aligned} Q(k) &\approx \hat{d}_2(\tilde{x}i_\gamma(k) + \tilde{y}v_\gamma^r(k)) - \hat{d}_1(\tilde{x}i_\delta(k) + \tilde{y}v_\delta^r(k)) \\ &= \hat{d}_2(\tilde{x}i_\gamma(k) + \tilde{y}v_\gamma(k)) - \hat{d}_1(\tilde{x}i_\delta(k) + \tilde{y}v_\delta(k)) \\ &\quad + \hat{d}_2\tilde{y}D_\gamma(k)V_{\text{dead}}(k) - \hat{d}_1\tilde{y}D_\delta(k)V_{\text{dead}}(k). \end{aligned} \tag{43}$$

Because the D_γ and D_δ are six-times fundamental-frequency components, for the HSPMSM drives, they can be filtered out easily through a low-pass filter. With the attenuation of the low-pass filter, the Q is obtained as

$$\begin{aligned} Q(k) &= \hat{d}_2(\tilde{x}i_\gamma(k) + \tilde{y}v_\gamma(k)) - \hat{d}_1(\tilde{x}i_\delta(k) + \tilde{y}v_\delta(k)) \\ &\quad - \hat{d}_1\tilde{y}\overline{D}_\delta(k)V_{\text{dead}}(k) \end{aligned} \tag{44}$$

where the $\overline{D}_\delta(k)$ is the direct component of the $D_\delta(k)$. In that case, the variation of Q from t_0 to t_1 is

$$\Delta Q = \hat{d}_2(\tilde{x}\Delta i_\gamma + \tilde{y}\Delta v_\gamma) - \hat{d}_1(\tilde{x}\Delta i_\delta + \tilde{y}\Delta v_\delta). \tag{45}$$

It can be observed that the ΔQ does not contain any V_{dead} items and thus the inverter nonlinearity has no effects on the proposed inductance identification method. The low-pass filter is designed as

$$G(z) = \frac{\omega_c T}{z - 1 + \omega_c T} \tag{46}$$

where the ω_c is the cutoff frequency. For the HSPMSM drives, the fundamental frequency is usually larger than 600 Hz, and thus, the frequency of the voltage distortion is up to 3.6 kHz. Therefore, without loss of generality, the cutoff frequency is selected as 500 Hz in this article.

C. Comparison With Conventional Method

In the conventional current-injection methods [29]–[31], with the current injection, the voltage equations are full-ranked and the system parameters can be calculated. In this article, the full-ranked equations are established as (16)

$$\begin{aligned} \Delta v_\gamma &= \frac{1}{y}(\cos(\omega T) - x)\Delta i_\gamma \\ \Delta v_\delta &= \frac{1}{y}\sin(\omega T)\Delta i_\gamma. \end{aligned} \tag{47}$$

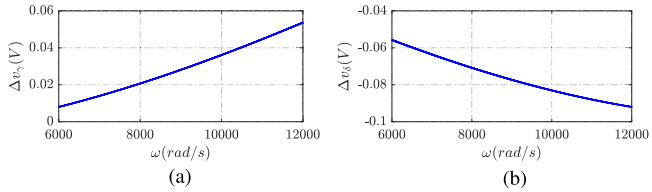

Fig. 6. Numerical results of the Δv_γ and Δv_δ with $\Delta i_\gamma = -0.4\,A$.

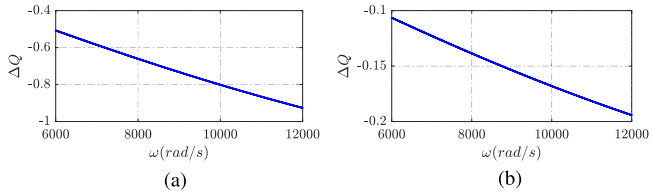

Fig. 7. Numerical results of the ΔQ with $\Delta i_\gamma = -0.4\,A$.

By solving this equation, there is

$$\begin{aligned} y &= \frac{\sin(\omega T)}{\Delta v_\delta}\Delta i_\gamma \\ x &= \cos(\omega T) - \frac{\Delta v_\gamma}{\Delta v_\delta}\sin(\omega T). \end{aligned} \tag{48}$$

According to the obtained x and y, the inductance can be derived as

$$\hat{L} = -\frac{1-x}{y}\frac{T}{\ln x}. \tag{49}$$

It can be observed that the estimation performance is based on the solution of the x and y. Therefore, the estimation accuracy relies on the Δv_γ and Δv_δ.

Fig. 6 shows the numerical results of the Δv_γ and Δv_δ with $\Delta i_\gamma = -0.4\,A$. Both the Δv_γ and Δv_δ are less than 0.1 V. Especially, for the Δv_γ, when $\omega < 10\,000$, it is smaller than 0.04 V, which is easily polluted by the system noise (resulting from measurement and nonlinearity of the inverter). In that case, the conventional estimation method may fail (refer to the experimental results). In the proposed method, as shown in Fig. 7, the ΔQ has a larger absolute value because of the large η, which improves the robustness against the system noise. Correspondingly, it provides a possibility to estimate the inductance with a very small injected current. It is an important improvement of the proposed method, as the main contribution of this article.

V. Validation and Analysis

In this section, the simulation performed in MATLAB/Simulink and experiments are designed to validate the effectiveness of the proposed inductance identification method. A simple proportional-integral (PI) controller is used in the speed loop. The system structure of the HSPMSM drive with proposed method is shown in Fig. 1. The experimental setup and the flowchart of the proposed method is shown in Fig. 8. The parameters of the tested HSPMSM are the same as shown in Table I. A fan is installed on the shaft of the test motor as a load, and thus, the load torque is approximately proportional

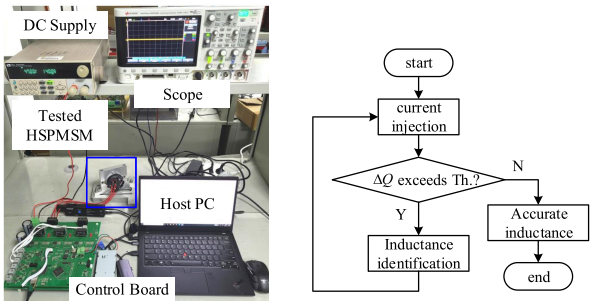

(a) (b)

Fig. 8. Experimental setup and flowchart of the proposed method.

TABLE I
PARAMETERS OF THE TESTED HSPMSM

Symbol	Parameter	Value
R	Winding resistance	0.023Ω
L	Stator inductance	23.5μH
U_{DC}	DC bus voltage	48V
I_N	Rated current	30A
$poles$	Rotor poles	2
f_s	Switching frequency	10kHz
T	Sampling period	100μs
n_N	Rated speed	100 kr/min
Ψ	Flux of the PM	0.0014Wb

TABLE II
q-AXIS CURRENT AT DIFFERENT SPEEDS

Speed	q-axis current
60 kr/min	10A
80 kr/min	18A
100 kr/min	30A

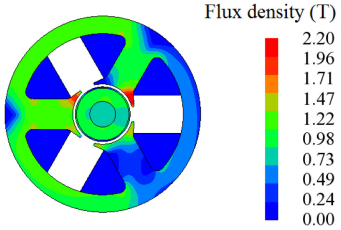

Fig. 9. Flux distribution of the tested HSMPSM at the rated condition.

to the square of the motor speed, as shown in Table II. All the experimental data are sent to the host PC by the Ethernet module in the control board.

A. Real Motor Inductance and Real Position Validation

Fig. 9 shows the flux distribution of the tested HSMPSM at the rated condition. It can be observed that the tested machine is not saturated at the rated condition, which is a common feature of HSPMSMs to reduce the iron losses [35]–[37]. In that case, the machine works under the linear region and the inductance is unchanged at different conditions.

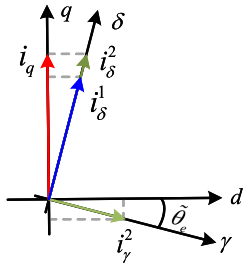

Fig. 10. Current vector diagram with current injection.

In order to evaluate the position estimation accuracy with the finite-element-method (FEM) inductance adopted, a current-injection validation is implemented, as shown in Fig. 10. During the injection, the speed controller still works to maintain the speed. Because of the same load, the q-axis current has to be same and there is

$$i_\delta^1 \cos\tilde{\theta}_e = i_\delta^2 \cos\tilde{\theta}_e - i_\gamma^2 \sin\tilde{\theta}_e \tag{50}$$

where the i_δ^1 is the δ-axis current value with the $i_\gamma = 0$ and the i_δ^2 is the the δ-axis current value with a positive i_γ^2 injected. Therefore, the estimation error can be calculated as

$$\tilde{\theta}_e = -\text{atan}\left(\frac{i_\delta^1 - i_\delta^2}{i_\gamma^2}\right). \tag{51}$$

Fig. 11 shows the i_δ performance and its fast-Fourier-transformation (FFT) analysis with mismatched inductance (0.7 and 1.3 L) adopted in the position estimation observer when a $+5$ A stepping current is injected into the γ axis at 60 and 100 kr/min. As is well known, only the direct component of the q-axis current produces torque. To illustrate the variation of i_δ, the FFT analysis before the injection and after the injection is also provided. In Fig. 11(a), with the injected γ-axis current, the i_δ decreases from 10.06 to 9.762 A. Based on (51), the estimation error can be calculated as -0.06 rad (i.e., $-3.41°$). At 100 kr/min, as shown in Fig. 11(b), with the injected γ-axis current, the i_δ decreases from 30.36 A to 29.67 A. The position estimation error can calculated as -0.137 rad (i.e., $-7.86°$). For the cases under 1.3 L, as shown in Fig. 11(c) and (d), the position estimation error at 60 and 100 kr/min can calculated as 0.057 and 0.155 rad (i.e., 3.26° and 8.87°), respectively.

Fig. 12 shows the i_δ performance with FEM inductance adopted in the position estimation observer when a $+5$ A is injected into the γ axis at 60, 80, and 100 kr/min, respectively. In Fig. 12(a), with the injected γ-axis current, the i_δ decreases from 9.94 to 9.86 A. Based on (51), the estimation error can be calculated as -0.016 rad (i.e., $-0.92°$). As shown in Fig. 12(b) and (c), the position estimation error at 80 and 100 kr/min can calculated as -0.016 and -0.02 rad (i.e. $-0.92°$ and $-1.146°$), respectively.

Therefore, according to these experimental results, the estimated rotor position with the FEM inductance is with high accuracy, and thus, it indicates that

1) the FEM inductance can be regarded as the real value;
2) the estimated rotor position with the FEM inductance can be treated as the real rotor position.

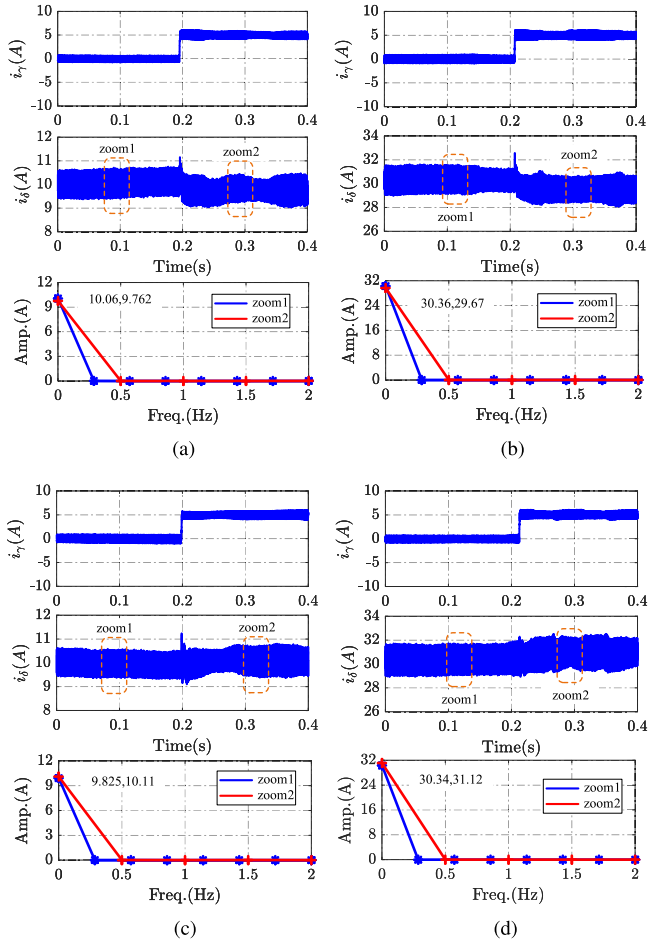

Fig. 11. Experimental results: i_δ and FFT analysis with mismatched inductance (0.7 L and 1.3 L) when a $+5$ A stepping current is injected into the γ axis. (From top to down: i_γ, i_δ, and FFT analysis of i_δ.

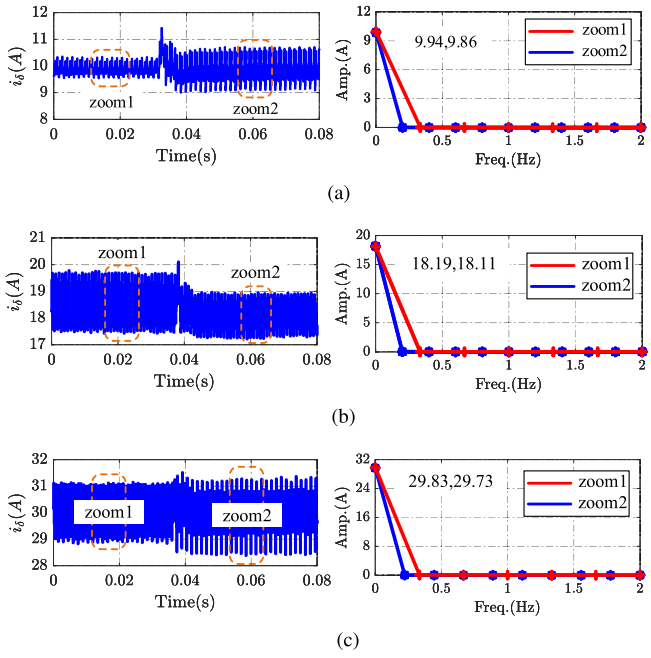

Fig. 12. Experimental results: i_δ and FFT analysis with FEM inductance when a $+5$ A stepping current is injected into the γ axis at 60, 80, and 100 kr/min.

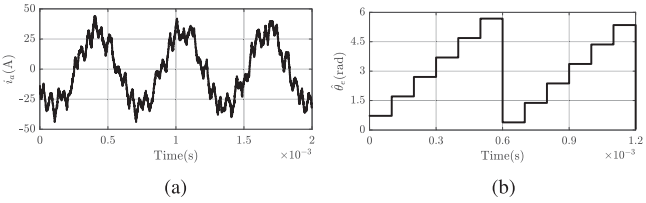

Fig. 13. Experimental results: phase A current i_a and the estimated position $\hat{\theta}_e$ at 100 kr/min.

B. Condition Check and Injected Current Selection

Besides, because the installation of the position sensor is difficult considering the reliability and the mechanical limitation, the experimental real rotor position is obtained by a back-EMF observer with the accurate parameters adopted.

When the parameters (R and L) varies 30% of their real values and the lowest speed is 6000 rad/s, the minimum φ is

$$\min(\varphi) = \varphi_{\hat{R}=1.3R,\hat{L}=1.3\,L,\omega=6000} = 56\,600 \tag{52}$$

and

$$\max\left(\frac{20}{\hat{L}I_N}\right) = \left(\frac{20}{\hat{L}I_N}\right)_{\hat{L}=0.7\,L} = 40\,527. \tag{53}$$

Therefore, the implementation condition is always satisfied.

In the experiments, without loss of generality, the following cases are considered.

1) Case 1: $\hat{R} = 1.3R$ and $\hat{L} = 0.7\,L$.
2) Case 2: $\hat{R} = 0.7R$ and $\hat{L} = 1.3\,L$.

Based on (40), in case 1, the injected current should meet

$$0.1352 < |\Delta i_\gamma| < 0.6. \tag{54}$$

In case 2, the injected current should meet

$$0.2212 < |\Delta i_\gamma| < 0.6. \tag{55}$$

Therefore, the Δi_γ is selected to 0.4 $A(1.33\%I_N)$.

Fig. 13 shows the experimental results of phase A current i_a and the estimated position $\hat{\theta}_e$ at 100 kr/min. Because of the 10-kHz switching frequency, the ratio of the switching/fundamental frequency is down to 6.

C. Performance With Different Speed

To validate the effectiveness of the proposed method at different speed, the experiments are established at 60 and 100 kr/min, respectively.

1) Simulation Results: Fig. 14 shows the simulation results with case 1 at 60 and 100 kr/min, respectively. In Fig. 14(a), at 0.05 s, a negative current (-0.4 A) is injected into the γ axis. Then the Q, which comes from the estimated δ-axis back-EMF $\hat{e}_\delta$ has a sharp decrease because of the mismatched inductance, which is consistent with the theoretical analysis mentioned above. By calculating the ΔQ, the inductance identification works based on (21) and the $\hat{L}$ increases to 23.52 μH ($L =$ 23.5 μH). The estimation error is approximately 0.02 μH. At around 0.08 s, another negative current (-0.4 A) is injected into the γ axis. The Q has a little increase, but it does not exceed the predefined threshold (0.02). With the estimated inductance

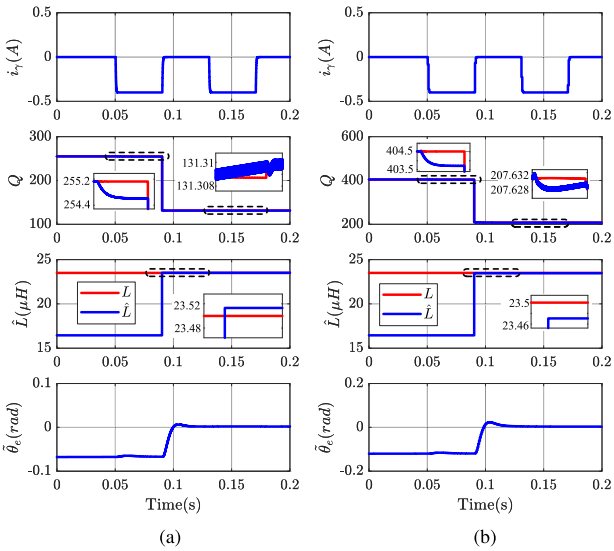

Fig. 14. Simulation results: performance of the proposed method with case 1. $\Delta i_\gamma = -0.4\,A$ (From top to down: i_γ, Q, $\hat{L}$, and $\tilde{\theta}_e$).

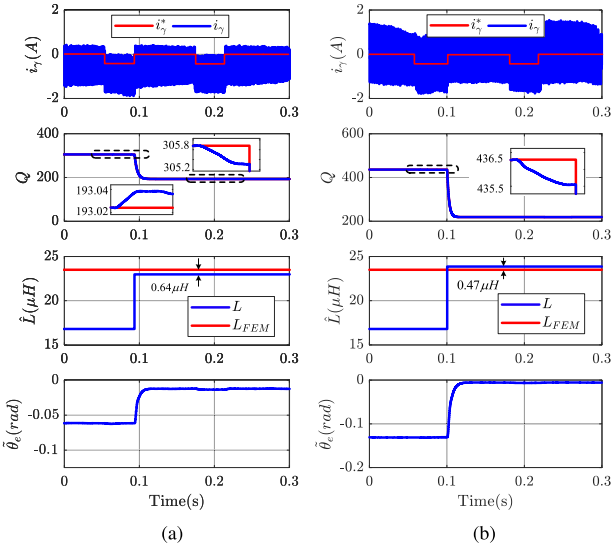

Fig. 15. Experimental results: Performance of the proposed method with case 1. $\Delta i_\gamma = -0.4$ A. (From top to down: i_γ, Q, $\hat{L}$, and $\tilde{\theta}_e$).

adopted in the back-EMF observer, the estimation error of the rotor position has been decreased to near zero. Fig. 14(b) shows the performance of the proposed method at 100 kr/min. The same procedure is operated and finally, the estimation error of the inductance is around $0.03\,\mu$H.

2) Experimental Results: Fig. 15 shows the experimental performance of the proposed inductance identification with case 2 at 60 and 100 kr/min, respectively. As demonstrated in Fig. 15(a), after the identification, the $\hat{L}$ is much close to the real inductance. The estimation error of the inductance is about $0.64\,\mu$H. At 100 kr/min as shown in Fig. 15(b), the estimation error of the inductance is reduced to $0.47\,\mu$H.

Fig. 16 shows the performance of the proposed method with case 2 at 60 and 100 kr/min. Finally, the estimation errors of

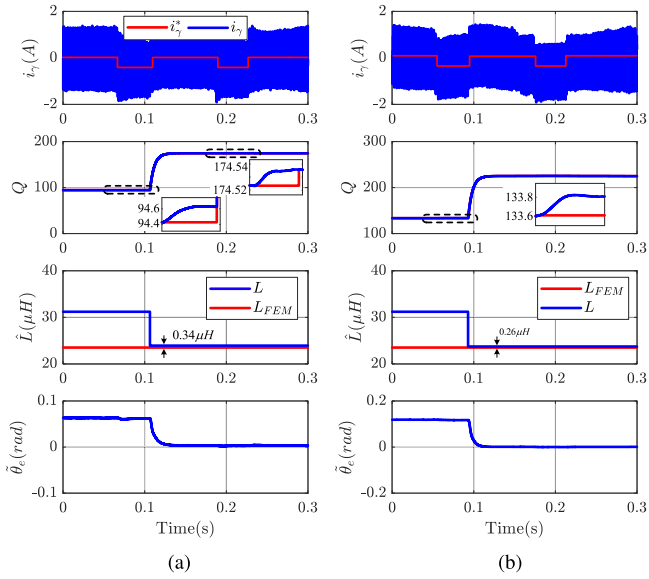

Fig. 16. Experimental results: Performance of the proposed method with case 2. $\Delta i_\gamma = -0.4$ A. (From top to down: i_γ, Q, $\hat{L}$, and $\tilde{\theta}_e$).

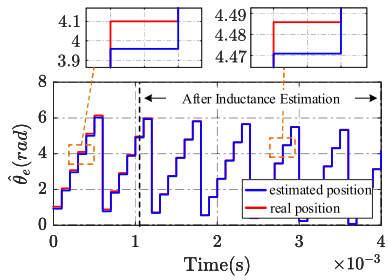

Fig. 17. Experimental result: Compensation performance of the position estimation error at 100 kr/min under case 1.

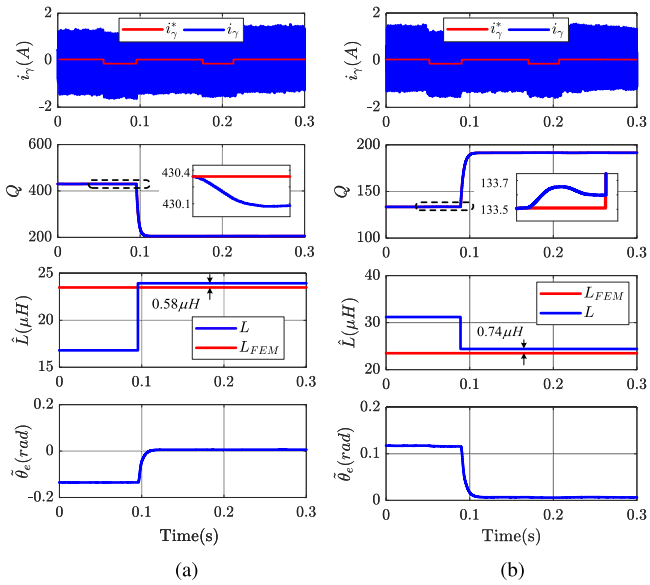

Fig. 18. Experimental results: performance of the proposed method with case 1 and case 2. $\Delta i_\gamma = -0.15$ A.

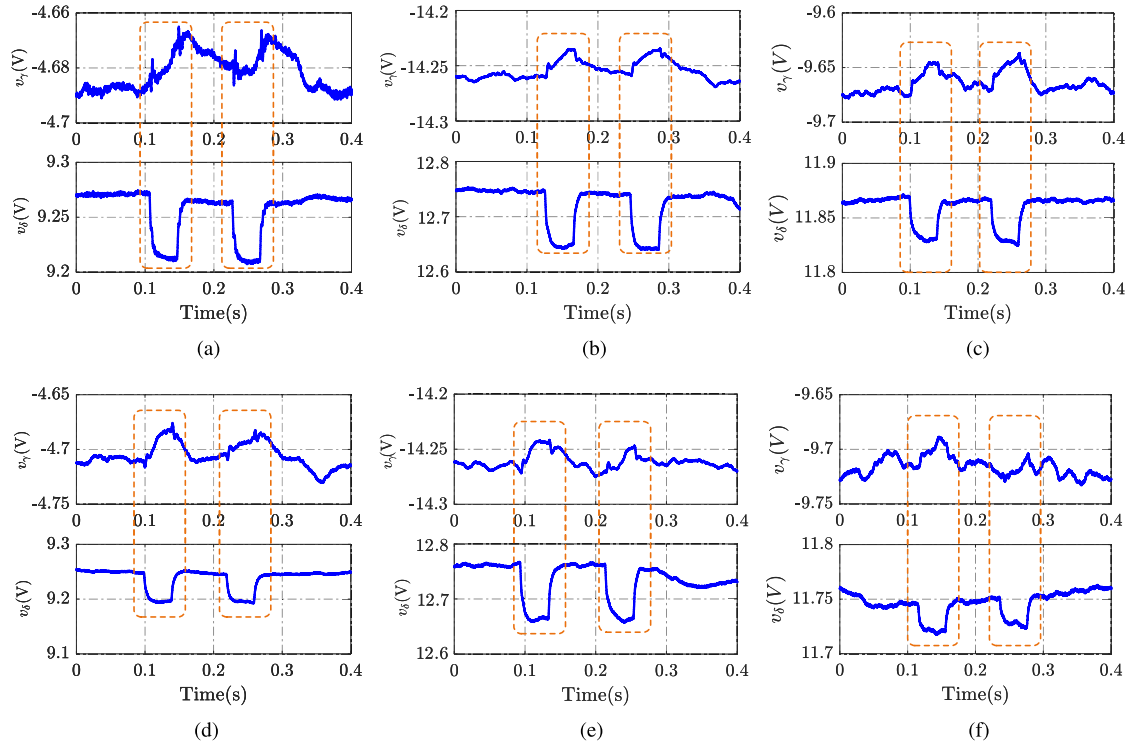

Fig. 19. Experimental results: Variation of the v_γ and v_δ of the proposed method with case 1 and case 2.

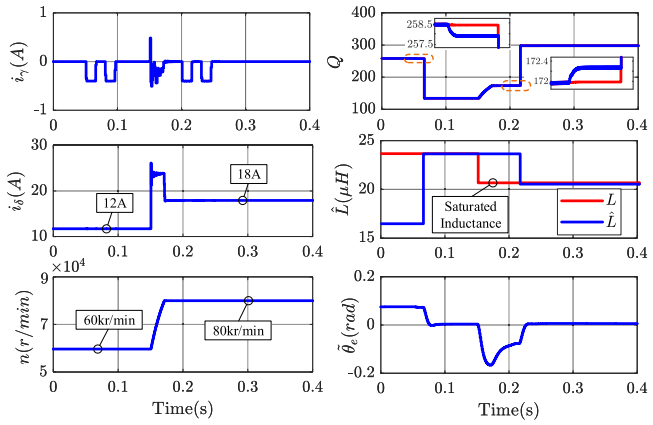

Fig. 20. Simulation results: Inductance saturation tracking performance with the proposed method.

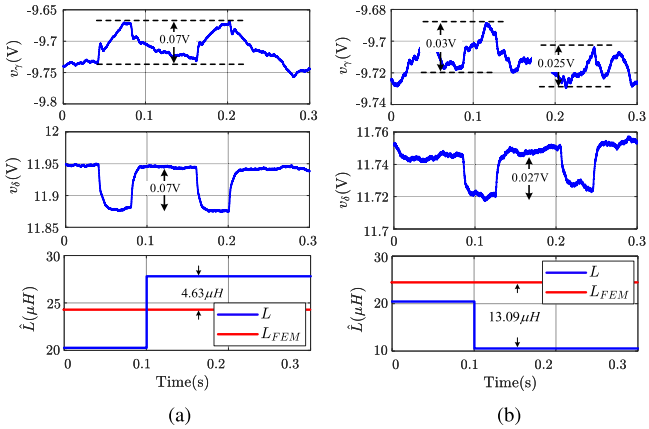

Fig. 21. Experimental results: The estimation performance of the conventional method (48) and (48) with $\Delta i_\gamma = -0.4$ A, 0.15 A at 80 kr/min.

the inductance have converged to 0.34 and 0.26 μH, respectively. Therefore, according to the simulation and experimental results, the inductance estimation error is limited within $\pm 5\%$ (1.175 μH) of the real value when the nominal resistance and inductance vary $\pm 30\%$ of their real values. The position estimation error can be reduced within 0.04 rad.

Fig. 17 shows the compensation performance of the position estimation error at 100 kr/min under case 1. With the mismatched parameter, the position estimation error is up to around -0.14 rad. After the inductance estimation, the estimation error is reduced to less than -0.02 rad, which has been well compensated.

D. Small Injected Current

Fig. 18 shows the experimental results of the proposed method with case 1 and case 2. $\Delta i_\gamma = -0.15$ A. With the small injected current ($0.5\% I_N$), the $|\Delta Q|$ is still up to 0.28 and 0.1 because of the large η. The estimation error of the inductance is around 0.5 and 0.74 μH, respectively. With the estimated inductance, the position estimation error is well compensated. Therefore, the effectiveness of the proposed method is still guaranteed with a small injected current (0.15 A).

Fig. 19 shows the variation of the v_γ and v_δ of the proposed method with case 1 and case 2. To illustrate the voltage variation clearly, the voltages are obtained by a low-pass filter and the

cutoff frequency is 200 Hz. When the $\Delta i_\gamma = -0.4\,\text{A}$, both the Δv_γ and Δv_δ are less than 0.15 V. Especially when the $\Delta i_\gamma = -0.15\,\text{A}$ is adopted, both the Δv_γ and Δv_δ are less than 0.05 V. Therefore, the proposed current-injected-based inductance identification method has negligible effect on the voltage margin of the drive system, which is the main contribution of this article.

E. Performance With Inductance Saturation

As the description mentioned above, the stator inductance of the HSPMSM will not be saturated because of the limitation of the iron losses. To validate the effectiveness of the tracking saturated inductance ability, a saturated HSPMSM is established in the simulation. In Fig. 20, when the speed varies from 60 to 80 kr/min, the q-axis current increases and the inductance saturation occurs. It can be concluded that the proposed inductance identification method can well track the inductance variation.

F. Comparison With Conventional Method

A comparison between the traditional current injection-based method and the proposed parameter identification method is also investigated.

Fig. 21(a) shows the experimental results of v_γ and v_δ with $\Delta i_\gamma = -0.4\,\text{A}$ at 80 kr/min. It should be noted that the voltages are obtained by a low-pass filter and the cutoff frequency is 200 Hz. From the observation, $\Delta v_\gamma = 0.07\,\text{V}$ and $\Delta v_\delta = -0.07\,\text{V}$. Based on (48) and (49), it can be calculated that $\hat{L} = 28.13\,\mu\text{H}$. The inductance estimation error can be $4.63\,\mu\text{H}$ (19.7%L), which resulting from the system noises of the v_γ.

Fig. 21(b) shows the experimental results of v_γ and v_δ with $\Delta i_\gamma = -0.15\,\text{A}$ and case 1 at 80 kr/min. With the small injected current ($0.5\%I_N$), the v_γ suffers from the system noises and it is difficult to obtain the variation after the current injection. If $\Delta v_\gamma = 0.0275\,\text{V}$ and $\Delta v_\delta = -0.027\,\text{V}$, it can be calculated that $\hat{L} = 10.91\,\mu\text{H}$. Clearly, the inductance estimation fails because of the system noises.

VI. Conclusion

This article proposes a robust inductance estimation method for EMF-based position sensorless drive of HSPMSMs by using a small current injection to correct the position estimation error. There are some achievements as follows.

1) The inductance estimation error is limited within $\pm 5\%$ of the real value when the nominal resistance and inductance vary $\pm 30\%$ of their real values. With the estimated inductance, the position estimation error can be much reduced to less than 0.04 rad.
2) The proposed method has enhanced robustness against the system noises. It is effective to estimate the inductance with a small injected current (0.5% of the rated current), where the conventional method fails.
3) The proposed method can be used with the low sampling/fundamental frequency ratio (down to 6).

References

[1] D. Gerada, A. Mebarki, N. L. Brown, C. Gerada, A. Cavagnino, and A. Boglietti, "High-speed electrical machines: Technologies, trends, and developments," *IEEE Trans. Ind. Electron.*, vol. 61, no. 6, pp. 2946–2959, Jun. 2014.

[2] W. Zhao, S. Jiao, Q. Chen, D. Xu, and J. Ji, "Sensorless control of a linear permanent-magnet motor based on an improved disturbance observer," *IEEE Trans. Ind. Electron*, vol. 65, no. 12, pp. 9291–9300, Dec. 2018.

[3] D. Xiao, S. Nalakath, Y. Sun, J. Wiseman, and A. Emadi, "Complex-coefficient adaptive disturbance observer for position estimation of IPMSMs with robustness to DC errors," *IEEE Trans. Ind. Electron.*, vol. 67, no. 7, pp. 5924–5935, Jul. 2020.

[4] S. Chi, Z. Zhang, and L. Xu, "Sliding-mode sensorless control of direct-drive PM synchronous motors for washing machine applications," *IEEE Trans. Ind. Appl.*, vol. 45, no. 2, pp. 582–590, Mar. 2009.

[5] Z. Qiao, T. Shi, Y. Wang, Y. Yan, C. Xia, and X. He, "New sliding-mode observer for position sensorless control of permanent-magnet synchronous motor," *IEEE Trans. Ind. Electron.*, vol. 60, no. 2, pp. 710–719, Feb. 2013.

[6] T. Bernardes, V. F. Montagner, H. A. Gründling, and H. Pinheiro, "Discrete-time sliding mode observer for sensorless vector control of permanent magnet synchronous machine," *IEEE Trans. Ind. Electron.*, vol. 61, no. 4, pp. 1679–1691, Apr. 2014.

[7] D. Liang, J. Li, R. Qu, and W. Kong, "Adaptive second-order sliding-mode observer for PMSM sensorless control considering VSI nonlinearity," *IEEE Trans. Power Electron.*, vol. 33, no. 10, pp. 8994–9004, Oct. 2018.

[8] J. Choi, K. Nam, A. A. Bobtsov, A. Pyrkin, and R. Ortega, "Robust adaptive sensorless control for permanent-magnet synchronous motors," *IEEE Trans. Power Electron.*, vol. 32, no. 5, pp. 3989–3997, May 2017.

[9] S. Po-ngam and S. Sangwongwanich, "Stability and dynamic performance improvement of adaptive full-order observers for sensorless PMSM drive," *IEEE Trans. Power Electron.*, vol. 27, no. 2, pp. 588–600, Feb. 2012.

[10] D. Bao, X. Pan, Y. Wang, X. Wang, and K. Li, "Adaptive synchronous-frequency tracking-mode observer for the sensorless control of a surface PMSM," *IEEE Trans. Ind. Appl.*, vol. 54, no. 6, pp. 6460–6471, Nov. 2018.

[11] X. Wu *et al.*, "Enhanced position sensorless control using bilinear recursive least squares adaptive filter for interior permanent magnet synchronous motor," *IEEE Trans. Power Electron.*, vol. 35, no. 1, pp. 681–698, Jan. 2020.

[12] T. Michalski, C. Lopez, A. Garcia, and L. Romeral, "Sensorless control of five phase PMSM based on extended Kalman filter," in *Proc. 42nd Annu. Conf. IEEE Ind. Electron. Soc.*, 2016, pp. 2904–2909.

[13] H. Kim, M. W. Degner, J. M. Guerrero, F. Briz, and R. D. Lorenz, "Discrete-time current regulator design for AC machine drives," *IEEE Trans. Ind. Appl.*, vol. 46, no. 4, pp. 1425–1435, Jul. 2010.

[14] S. C. Yang and G. R. Chen, "High-speed position-sensorless drive of permanent-magnet machine using discrete-time EMF estimation," *IEEE Trans. Ind. Electron.*, vol. 64, no. 6, pp. 4444–4453, Jun. 2017.

[15] Y. Yao, Y. Huang, and F. Peng, "Position sensorless drive of high speed permanent magnet synchronous motor," in *Proc. IEEE Energy Convers. Congr. Expo.*, 2018, pp. 1733–1740.

[16] H. A. A. Awan, T. Tuovinen, S. E. Saarakkala, and M. Hinkkanen, "Discrete-time observer design for sensorless synchronous motor drives," *IEEE Trans. Ind. Appl.*, vol. 52, no. 5, pp. 3968–3979, Sep. 2016.

[17] S. J. Underwood and I. Husain, "Online parameter estimation and adaptive control of permanent-magnet synchronous machines," *IEEE Trans. Ind. Electron.*, vol. 57, no. 7, pp. 2435–2443, Jul. 2010.

[18] T. Boileau, N. Leboeuf, B. Nahid-Mobarakeh, and F. Meibody-Tabar, "Online identification of PMSM parameters: Parameter identifiability and estimator comparative study," *IEEE Trans. Ind. Appl.*, vol. 47, no. 4, pp. 1944–1957, Jul. 2011.

[19] W. Deng, C. Xia, Y. Yan, Q. Geng, and T. Shi, "Online multiparameter identification of surface-mounted PMSM considering inverter disturbance voltage," *IEEE Trans. Energy Convers.*, vol. 32, no. 1, pp. 202–212, Mar. 2017.

[20] D. Q. Dang, M. S. Rafaq, H. H. Choi, and J. Jung, "Online parameter estimation technique for adaptive control applications of interior PM synchronous motor drives," *IEEE Trans. Ind. Electron.*, vol. 63, no. 3, pp. 1438–1449, Mar. 2016.

[21] Z. Liu, H. Wei, Q. Zhong, K. Liu, X. Xiao, and L. Wu, "Parameter estimation for VSI-fed PMSM based on a dynamic PSO with learning strategies," *IEEE Trans. Power Electron.*, vol. 32, no. 4, pp. 3154–3165, Apr. 2017.

[22] S. Li, J. Fang, and B. Han, "High-precision parameter identification of high-speed magnetic suspension motor," *IEEE Trans. Energy Convers.*, vol. 33, no. 1, pp. 20–31, Mar. 2018.
[23] Y. Yao, Y. Huang, F. Peng, J. N. Dong, and H. Zhang, "An improved deadbeat predictive current control with online parameter identification for surface-mounted PMSMs," *IEEE Trans. Ind. Electron.*, vol. 67, no. 12, pp. 10145–10155, Dec. 2020.
[24] S. Ichikawa, M. Tomita, S. Doki, and S. Okuma, "Sensorless control of permanent-magnet synchronous motors using online parameter identification based on system identification theory," *IEEE Trans. Ind. Electron.*, vol. 53, no. 2, pp. 363–372, Apr. 2006.
[25] O. C. Kivanc and S. B. Ozturk, "Sensorless PMSM drive based on stator feedforward voltage estimation improved with MRAS multiparameter estimation," *IEEE/ASME Trans. Mechatronics*, vol. 23, no. 3, pp. 1326–1337, Jun. 2018.
[26] S. Ichikawa, M. Tomita, S. Doki, and S. Okuma, "Sensorless control of synchronous reluctance motors based on extended EMF models considering magnetic saturation with online parameter identification," *IEEE Trans. Ind. Appl.*, vol. 42, no. 5, pp. 1264–1274, Sep. 2006.
[27] A. Piippo, M. Hinkkanen, and J. Luomi, "Adaptation of motor parameters in sensorless PMSM drives," *IEEE Trans. Ind. Appl.*, vol. 45, no. 1, pp. 203–212, Jan. 2009.
[28] M. S. Rafaq, F. Mwasilu, J. Kim, H. H. Choi, and J. Jung, "Online parameter identification for model-based sensorless control of interior permanent magnet synchronous machine," *IEEE Trans. Power Electron.*, vol. 32, no. 6, pp. 4631–4643, Jun. 2017.
[29] K. Liu, Q. Zhang, J. Chen, Z. Q. Zhu, and J. Zhang, "Online multiparameter estimation of nonsalient-pole PM synchronous machines with temperature variation tracking," *IEEE Trans. Ind. Electron.*, vol. 58, no. 5, pp. 1776–1788, May 2011.
[30] K. Liu and Z. Q. Zhu, "Quantum genetic algorithm-based parameter estimation of PMSM under variable speed control accounting for system identifiability and VSI nonlinearity," *IEEE Trans. Ind. Electron.*, vol. 62, no. 4, pp. 2363–2371, Apr. 2015.
[31] G. Feng, C. Lai, K. Mukherjee, and N. C. Kar, "Current injection-based online parameter and VSI nonlinearity estimation for PMSM drives using current and voltage DC components," *IEEE Trans. Transport. Electrific.*, vol. 2, no. 2, pp. 119–128, Jun. 2016.
[32] X. Song, J. Fang, B. Han, and S. Zheng, "Adaptive compensation method for high-speed surface PMSM sensorless drives of EMF-Based position estimation error," *IEEE Trans. Power Electron.*, vol. 31, no. 2, pp. 1438–1449, Feb. 2016.
[33] J. Kim, I. Jeong, K. Nam, J. Yang, and T. Hwang, "Sensorless control of PMSM in a high-speed region considering iron loss," *IEEE Trans. Ind. Electron.*, vol. 62, no. 10, pp. 6151–6159, Oct. 2015.
[34] H.-S. Kim, K.-H. Kim, and M.-J. Youn, "On-line dead-time compensation method based on time delay control," *IEEE Trans. Control Syst. Technol.*, vol. 11, no. 2, pp. 279–285, Mar. 2003.
[35] T. Fan, Q. Li, and X. Wen, "Development of a high power density motor made of amorphous alloy cores," *IEEE Trans. Ind. Electron.*, vol. 61, no. 9, pp. 4510–4518, Sep. 2014.
[36] F. R. Ismagilov, N. Uzhegov, V. E. Vavilov, V. I. Bekuzin, and V. V. Ayguzina, "Multidisciplinary design of ultra-high-speed electrical machines," *IEEE Trans. Energy Convers.*, vol. 33, no. 3, pp. 1203–1212, Sep. 2018.
[37] G.-H. Jang, J.-H. Ahn, B.-O. Kim, D.-H. Lee, J.-S. Bang, and J.-Y. Choi, "Design and characteristic analysis of a high-speed permanent magnet synchronous motor considering the mechanical structure for high-speed and high-head centrifugal pumps," *IEEE Trans. Magn.*, vol. 54, no. 11, Nov. 2018, Art. no. 8204906.

Yu Yao (Student Member, IEEE) received the B.S. degree in electrical engineering, in 2016, from Southeast University, Nanjing, China, where he is currently working toward the doctor of engineering degree in electric machines and control with the School of Electrical Engineering.

His research interests include the design of the power inverter, the current regulator design, the position sensorless drive for the high-speed PSMSM and active damping methods for the high-speed drive system with *LCL* output filter.

Yunkai Huang received the M.Sc. and Ph.D. degrees in electrical engineering from the Southeast University, Nanjing, China, in 2001 and 2007, respectively.

He is currently a Professor with the School of Electrical Engineering, Southeast University. His research interests include design and control of PM machine and high speed machine, applications in domestic appliances, electric vehicles, railway traction, all-electric ships, more-electric aircraft, and wind power generation systems.

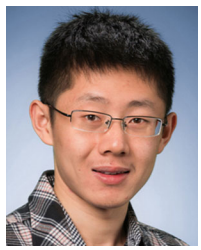

Fei Peng (Member, IEEE) received the B.S. and M.S. degree in electrical engineering from Southeast University, Nanjing, China, in 2010 and 2012, respectively. He received the Ph.D. degree in electrical and computer engineering from McMaster University, Hamilton, ON, Canada, in 2016.

After that he worked as a Postdoctoral Fellow with the McMaster Institute for Automotive Research and Technology (MacAUTO), McMaster University. From December 2016, he joined the School of Electrical Engineering at Southeast University, Nanjing, China, as an Assistant Professor. His research interests include optimal design and control of power converters, modeling and digital control of motor drives.

Jianning Dong (Member, IEEE) received the B.S. and Ph.D. degrees in electrical engineering from Southeast University, Nanjing, China, in 2010 and 2015, respectively.

He is an Assistant Professor with the Delft University of Technology, Delft, Netherlands, since 2016. Before joining TU Delft, he was a Postdoc Researcher with McMaster Automotive Resource Centre (MARC), McMaster University, Hamilton, ON, Canada. His research interests are design, modeling and control of electromechanical systems.

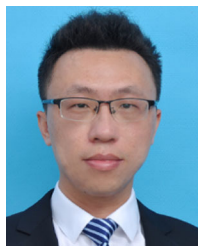

Zichong Zhu (Student Member, IEEE) received the B.S. degree in thermal energy and power engineering from Nanjing Institute of Technology (NJIT), Nanjing, China, in 2014, and the Ph.D. degree from Southeast University (SEU), Nanjing, China, in electrical engineering, China, in 2021, respectively.

He joined Nanjing Tech University, Nanjing, China, as a Lecturer, in 2021. His research interests include electromagnetic analysis, thermal management and structural design of the permanent magnet synchronous machines for the wheel-hub driving, turbo and servo applications.